Chapter 6

Discussion

The aim of this chapter is to collate and discuss the material and the results presented in previous chapters.

First, the mechanisms of colour production on the wings of *Morpho rhetenor* will be addressed. Based on the results of the experimental investigation of the butterfly microstructure and on the theoretical analysis of its periodic arrangement, the mechanisms behind the optical phenomenology that interested generations of scientist are explained through a study of the structural components of the microstructure. The validity of two-dimensional modelling is demonstrated and a model of the collective behaviour of said components is presented in detail. The relevance of the necessary approximations of the modelling is also discussed.

The fabricated two- and three-dimensional volume diffractive structures inspired by the *Morpho* microstructure are then discussed with attention to the opportunities and limitations of the fabrication technologies employed and to the optical properties of these devices.

6.1 The mechanisms of colour production on the wings of *Morpho rhetenor*

The scales covering the wings of the tropical butterfly *Morpho rhetenor* produce a striking colour display. Generation of the structural colour is obtained at the surface of the scales covering the wings through an intricate arrangement of chitin, the colourless, low-index dielectric material of which the scales are made. The chitin microstructure is periodic and consists approximately of a one-dimensional grating with tree-shaped diffractive elements. The vertical distribution of the diffractive elements is also regular with constant distance between and constant thickness of the branches. The height of the elements exceeds the lateral period and each element includes several vertical periods, which makes the microstructure comparable to man-made multilevel gratings or volume diffractive structures. The morphology of the scales and details about the geometrical dimensions of the microstructure have been presented in section 1.2.2. The regularity of the modulation of the dielectric material in the *Morpho* microstructure allows the theoretical study of its optical properties using methods employed in the modelling of photonic crystals (PCs). Figure 6.1 shows a TEM cross-section of the microstructure (left-hand side) and an example of model (right-hand side). This matter will be discussed

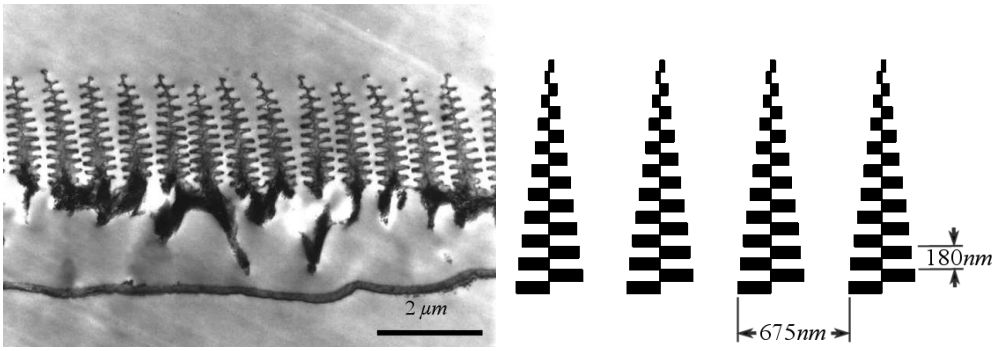

Figure 6.1: TEM micrograph showing the cross-section of a scale of *Morpho rhetenor* [17] (left-hand side). Example of a model of the *Morpho* microstructure (right-hand side).

further on in this chapter.

To date a complete characterisation of the optical properties of the *Morpho* microstructure has not been reported. In previous experimental investigations carried out on similar butterflies (class I) the characterisation was limited by a choice of specific conditions of incidence and collection, for example by the use of unpolarised light or a single wavelength, or by the investigation of specific angles of incidence only. However, from past measurements [17] three main properties of the *Morpho* microstructure emerged: (i) for normal incidence, it produces high reflections (up to 70% in total reflection); (ii) most of the reflected power is concentrated in the blue regime of the visible spectrum; (iii) for normal incidence and at a wavelength of $488nm$, the reflected power is distributed around two directions of scattering, each one at an angle of 30° with respect to the wing normal. Additionally, the measurement of the peak wavelength of the light reflected by another class I butterfly showed a shift towards shorter wavelengths with increasing angle of incidence, an effect equally expected to occur in *Morpho rhetenor*.

A preliminary analysis performed with photographic methods (cf. section 4.1) qualitatively confirmed the results obtained by other scientists and revealed the following key properties:

- Large portions of the wing have a distinct blue and green colour irrespective of the angle of incidence of the impinging light.
- At all angles of incidence the light is back-scattered over a wide range of angles extending at least 50° from the direction of specular reflection.
- A distinct if not dramatic change in hue is observed when filtering the back-scattered light with a linear polariser.

In order to quantify the perception of colour, we shall refer to the definition of the spectral content for the green and blue colours given by Stilles and Burchs [104] and called CEI standard observer colour matching functions, which are shown in figure 6.2. Green is found between 492 and $623nm$

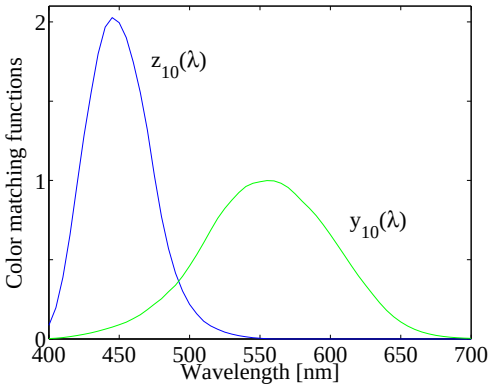

Figure 6.2: CIE standard observer color matching function for green (function $y_{10}(\lambda)$) and blue (function $z_{10}(\lambda)$) colours [104].

(1/e peak value thresholds) and blue between 416 and 481nm. These functions do not necessarily represent the definition of the colours used by the digital device mentioned above.

To substantiate the qualitative observations mentioned above, a novel measurement method was developed, which permits complete characterisation of the scattering of light by a sample for all wavelengths of the visible and near-infrared spectrum, and for all angles of incidence and polarisations. Instrumental for this method was the use of a photonic crystal fibre to generate a supercontinuum of coherent, white-light that could be focussed to a beam waist of 30μm. A purpose built goniometer was capable of aligning the optical axes of the incident and collected light with nanometer scale accuracy. Through appropriate gauging this method yielded absolute values of the measured light intensities. This experimental method was described in section 4.2.

The scattering properties of the *Morpho* microstructure were characterised in the reflection regime using the experimental setup. By means of a low-aperture beam, incident in the plane normal to the ridges of the microstructure at representative angles of incidence (10°, 30° and 60°), the back-scattered light intensity was measured with high angular resolution and low aperture of the collection on the entire hemicycle of the plane of inci-

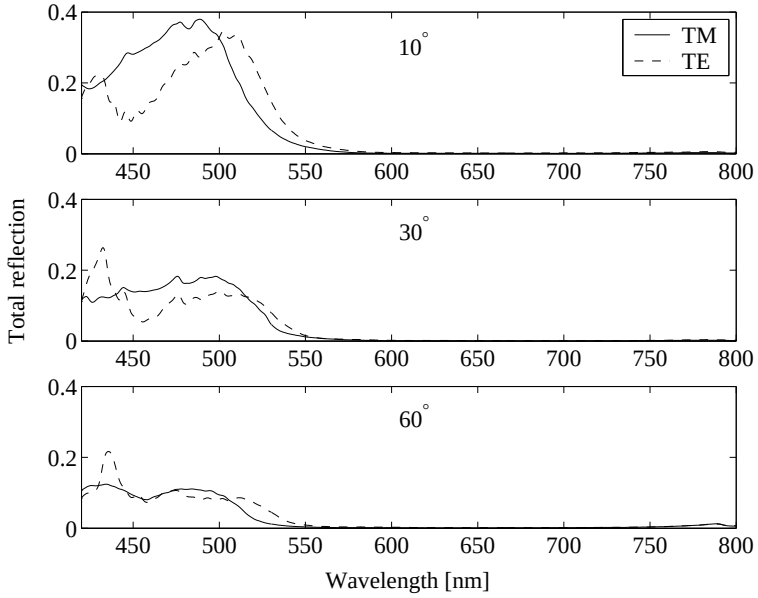

Figure 6.3: Total reflection of *Morpho rhetenor* microstructure for angles of incidence of 10°, 30° and 60°, and both polarisations.

dence, but for an arc extending ±10° from the direction of incidence (the blind spot). The capacity to focus all wavelengths of the white incident light to a very small spot allowed illumination of a small portion of a single scale, thus eliminating optical effects due the wing corrugation and the periodic tiling with scales. No substantial out-of-plane scattering was observed, thus confirming the essential two-dimensionality of the microstructure.

The following properties were determined from this investigation:

- At all angles of incidence included in the measurements the microstructure behaves as a low-pass filter with a long-wavelength threshold of the reflection band in the total reflection spectra approximately placed at 520 and 535nm for the TM and TE polarisations, respectively. By total reflection is meant the sum of all back-scattered light. Also, for TE polarised light, a transfer of power to shorter wavelengths with increasing angle of incidence was observed. The spectra of the total reflection are shown in figure 6.3.

- For TM polarised light total reflection maxima larger than 38%, 18% and 12% were measured for angles of incidence of 10°, 30° and 60°, respectively. For TE polarised light total reflections maxima larger than 35%, 26% and 21% were measured for angles of incidence of 10°, 30° and 60°, respectively.

- In comparison to other directions of propagation of the back-scattered light, the specular reflection was largely extinguished.

- No discernible polarisation mixing was found.

- For all angles of incidence, most of the reflected power propagated at angles less than 30° away from the angle of incidence. In other words, irrespective of the microstructure orientation, most of the back-scattered light was concentrated around the direction opposite to that of the incident beam, as if this was impinging normally onto a mirror. This effect can be observed in the spectrograms of figure 6.4

These properties agree with previously published results and with the photographic analysis, and depict a more detailed view of the optical phenomenology of the microstructure. The spectral content of the reflected light is mainly blue and has a considerable amount of green, which differs when changing polarisation. A deviation is noted in the maximum value of the total reflection from the data reported by Vukusic *et. al.* [17], which is due to the reduced measurement of the back-scattered power caused by the blind spot of the setup. The absence of any polarisation mixing confirms the intrinsic low dimensionality of the butterfly microstructure. The independent propagation of waves with orthogonal polarisations inside two-dimensional arrangements was discussed in section 2.1.1.

With these new results from the experimental investigation it is possible to expand our understanding of the physics involved in the phenomenology of the butterfly microstructure. The spectral content of the total reflection is dominated by the multilayered arrangement, a fact already acknowledged

by the earliest researchers. However, a change in angle of incidence does not produce the shift of the long-wavelength edge of the high-reflection band expected from a mere one-dimensional, multilayer arrangement. A comparison between the dependence of the edge on the angle of incidence for the *Morpho* microstructure and for a multilayer model is shown in figure 6.5. The wavelength at which the $1/e$ drop in the plateau power is measured was at $(535 \pm 2)nm$ for all angles of incidence. On the other hand, the position of the edge for the multilayer model shifts from $525nm$ to $440nm$ when increasing the angle of incidence from 10° to 60°. A distribution of dielectric mirrors oriented around two directions, at ±15° from the scale normal, was

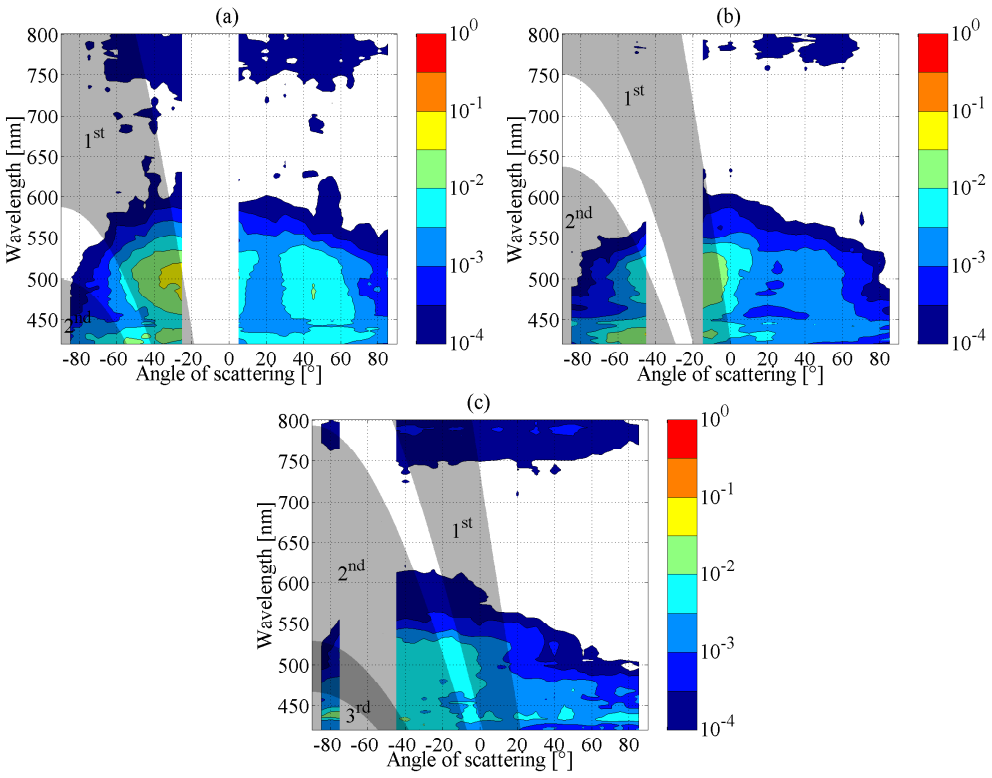

Figure 6.4: Filled contour plots of the scattering from the surface of the wings of *Morpho rhetenor* at different angles of incidence and for TE polarisation. (a) 10° incidence, (b) 30° incidence, (c) 60° incidence. The grey areas correspond to the orders of diffraction for lateral periods varying between 500 and $850nm$ ($(675 \pm 175)nm$) and are labelled with their order number.

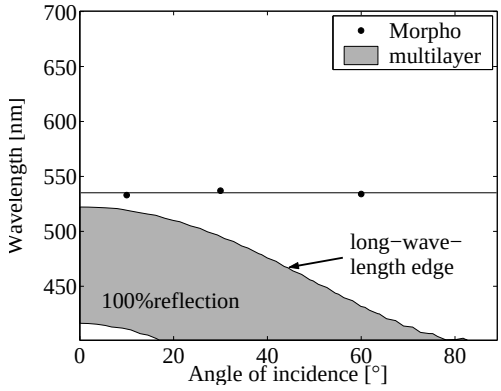

Figure 6.5: Comparison between the dependence of the long-wavelength edge of the high-reflection band on the angle of incidence for the *Morpho* microstructure and a multilayer model. On the coordinate axes are the angle of incidence and the wavelength of the impinging light. Dots indicate the measured threshold wavelength ($1/e$ of plateau power) for TE polarisation. The line is drawn for illustration purposes. The gray area is a filled contour plot of the high-reflection band of a stack of ten $90nm$-thick layers of chitin (index of refraction 1.56) interspaced with $90nm$-thick layers of air for the TE polarisation. These values were computed with the TMM presented in appendix C.

proposed by Vukusic *et. al.* [17] and successfully accounted for the formation of two equal lobes symmetrically arranged around the scale normal in the polar plots of the scattering of monochromatic light impinging at normal incidence. However, it is not possible to extend the validity of such a model to describe the scattering of light at non-normal incidence. In fact, the measured progressive extinction of the power scattered into the second lobe with increasing angle of incidence cannot be accounted for by this model. This phenomenon is illustrated in figure 6.4. The ratios of the maximum intensities of the two lobes measured for TE polarisation are 23% and 9% for angles of incidence of 10° and 30°, respectively. Under these conditions of incidence, corresponding to angles of incidence of 25° and 45° for the central mirrors responsible for the weaker lobe in Vukusic's model, no reduction of the reflected intensity is expected.

In view of the marked periodicity observed from TEM micrographs of

the cross-section of the *Morpho* microstructure, grating-type periodic models have been investigated. An average value of the period and its variance was extracted from microscopy data including only few periods, while the measured spectra were obtained illuminating an area extending over several hundred periods. A targeted study to establish these figures is necessary to validate the proposed models and is included in the propositions for future work in the conclusion.

The theoretical study of periodic models of the microstructure has permitted one to identify the possible role of different features observed in the microstructure for the generation of its response in the reflection regime. With models based on arrangements of chitin periodic in two orthogonal directions, it was possible to apply modelling techniques used for PCs. From the micrograph shown on the left-hand side of figure 6.1 it was established that a model as the one shown on the right-hand side of the same figure included an interesting geometrical aspect of the structure of each tree-shaped element: the phase shift between branches on opposed sides of the central stalk. Due to the irregular bending of the trees however, the branches are often arranged symmetrically. These particular arrangements fall within two special *Bravais* lattices defined in two-dimensional crystallography [88]: a rectangular lattice and a centred rectangular lattice. The theory of two-dimensional PCs presented in sections 2.1.3 and 2.1.4 has shown that for both a rectangular and a centred rectangular lattice of rectangular elements, having the same index of refraction of chitin, and periods and an area filling fraction drawn from average values of the butterfly microstructure, gaps occur between bands belonging to neighbouring *Brillouin* zones. This is a well known property of photonic bandgap materials and manifests in high-reflectivity bands for frequencies within the gap [33, 43, 44, 45]. For illustrative purposes, the band diagram of one computed structure is shown in the plot on the left-hand side of figure 6.6, while the bandgap between the lowest band and the band of one neighbouring *Brillouin* zone is shown on the right-hand side of the same figure. This bandgap overlaps part of the visible spectrum for both polar-

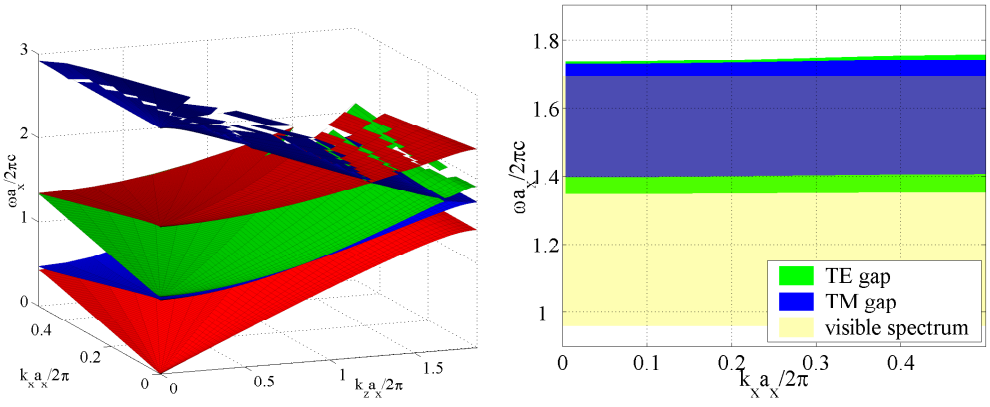

Figure 6.6: Band diagram (left-hand side) of the rectangular structure discussed in section 2.1.3 and lowest bandgap between neighbouring *Brillouin* zones for the same structure (right-hand side).

isations, including all wavelengths from $400nm$ up to the long-wavelength threshold of the respective bandgaps. The reader is referred to chapter 2 for details about the method of computation, the geometry of the structures and results. For the rectangular lattice, the bandgap occurring in the first *Brillouin* zone is at wavelengths shorter than 504 and $485nm$ for the TE and TM polarisations, respectively. For the centred rectangular lattice, these thresholds are at 469 and $434nm$. In all cases, the long-wavelength edge of this bandgap is flat, *i.e.* it does not vary with a change of the tangential component of the wave vector, as it is illustrated by the lower limits of the bandgaps shown in the plot on the right-hand side of figure 6.6. A variation of the crystal dimensions shifts the thresholds linearly with the scaling factor. This is easily appreciated considering the plots of figure 6.6, where all values on the axes are scaled to the parameter a_x. The results of the computations do not depend on the absolute sizes of the structures, but only on the ratio between frequency and reciprocal lattice constants. A change in a_x causes the values of the band edge to vary accordingly. Considering the collective properties of a distribution of crystals with different dimensions that can be qualitatively seen as a set of the same structure with different scaling factors, a smearing of the threshold edges is obtained.

The properties of the bulk PCs related to the bandgap at the far end of the first *Brillouin* zone, such as low-pass filter behaviour in the visible spectrum, polarisation dependence, and independence from the angle of incidence, agree with the experimental data presented above (figure 6.3). The stability of the edge of the high-reflection band with changing angle of incidence shows that, irrespective of the condition of incidence, a considerable amount of power is consistently coupled to the modes of the first *Brillouin* zone. This property is due to the tapering of the crystals and can be qualitatively accounted for using the results of the band diagram study. Reducing the area filling fraction of the crystal diminishes the average index of refraction of the material and makes all bands steeper, thus pushing all bands to higher frequencies except for the first one. The steepening of the first band and the resulting shift of the long-wavelength bandgap edge to shorter wavelengths with decreasing linear filling fraction f_x along the direction of the long period is shown in figure 6.7. A wave with wavelength in the visible spectrum impinging on a crystal with low filling fraction, such as the top surface of the tapered crystal, can only couple to the first band. The theory of infinitely extended arrangements, on which these observations are based, however cannot account for the diffraction at the surface of a periodic structure.

To substantiate these views on the mechanisms of colour production, the diffraction of two-dimensional models of the *Morpho* microstructure were studied using a novel computational method. Progress in the modelling of the optical properties of diffractive structures have shown that the use of rigorous, vectorial methods is necessary to compute the diffraction efficiencies of deep gratings operating in a regime of wavelengths comparable to the period of the distributions (zero-order gratings).

To compute the diffraction of models of the butterfly microstructure, a state-of-the-art numerical method was developed, which incorporated FDTD and NFFFT algorithms. This method and its application to the study of dielectric structures is presented in chapter 5. The numerical modelling con-

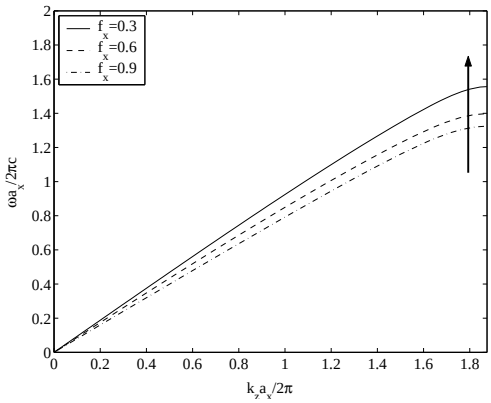

Figure 6.7: First band for rectangular structures with different filling fractions along the direction of the long period f_x and constant filling fraction in the perpendicular direction ($f_z = 0.5$). The computation was performed for TM polarised waves with the method described in section 2.1.3.

firmed the following optical properties of the *Morpho* microstructure:

- The low-pass filter behaviour with a threshold of the high-reflection band edge independent from the angle of incidence.
- The high maxima of total reflection, with values larger than 90% for some of the models.
- The extinction of the specular reflection.
- The transfer of the reflected power into the higher orders of diffraction with growing angle of incidence, resulting in back-scattering of light in the directions closer to the direction of incidence.

With this tool a comparative study of the reflection and diffraction properties of features occurring in the *Morpho* microstructure was carried out. Four structures were analysed: (a) a rectangular lattice of rectangular dielectric elements; (b) a tapered version of the above, resulting in a pine tree structure with its tips towards the incident front; (c) a centred rectangular lattice of rectangular dielectric elements; and (d) a tapered version of (c),

resulting in an asymmetric pine tree structure. Schematic views of these arrangements of dielectric are shown in figure 5.5. The following conclusions were drawn from this study:

- All of the structures show a high-reflection band at short wavelengths in the visible spectrum and the position in the spectrum of its long-wavelength edge does not change with varying angle of incidence.

- For the structures with a centred rectangular lattice (c and d) the 0^{th} order (or specular reflection) is largely extinct (completely for the tapered type d) for all angles of incidence when compared to the rectangular structures (a and b). Consequently, the reflected power is distributed amongst other diffraction orders.

- For both lattices, the tapering extinguishes the long-wavelength low-intensity peaks of the straight structures, thus generating a perfect low-pass filtering behaviour. The tapering also smoothes local modulation of the spectra and consequently only wide peaks occur in the spectra. Additionally, the tapering in structures with a rectangular lattice enhances the transfer of power to the 1^{st} order of diffraction for TM polarised light in comparison to the straight ones.

The results of the numerical study are consistent with the properties emerging from the analysis of the band structure of rectangular and centred rectangular lattices mentioned above. The finiteness of the structures in the numerical study caused a shift of the long-wavelength edges of the high-reflection bands due to the presence of side peaks, an effect also normally occurring with multilayer stacks. The position of the edge for the straight rectangular structures is within $10nm$ of the measured threshold. It was shown in section 5.2 that a change in the lateral period does not affect the position of the long-wavelength edge of the high-reflection band. On the other hand, the position of the threshold scales linearly with the vertical period.

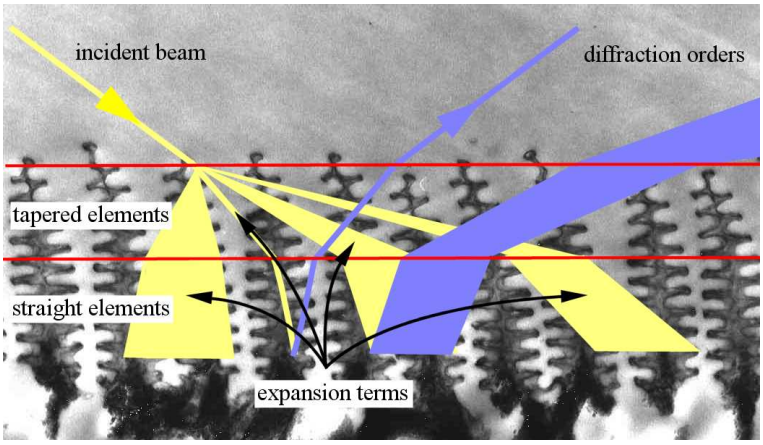

Figure 6.8: Illustration of the two-layer model of the *Morpho* microstructure with superimposed expansion terms of a propagating mode and resulting diffraction orders. A distribution of lateral periods causes a spread in the directions of propagation of waves inside and outside the microstructure.

The properties of the studied structures suggest that it is possible to construct a model which accounts qualitatively for the observed properties of the *Morpho* microstructure. Let us consider a model in which the light impinges on a mixture of tapered rectangular and centred rectangular structures, as illustrated in figure 6.8, and then propagates into the structure to find an arrangement with straight elements. The tapered layer acts as an effective low-pass filter with high efficiencies in the 1^{st} order of diffraction. The power of the transmitted radiation is transferred into the underlying mixture of rectangular and centred rectangular straight structures. With most of the propagating power coupled to the first band due to the low filling fraction of the top surface, the bandgap of the first *Brillouin* zone edge of the bottom layer reflects efficiently the propagating power for any angle of propagation of the mode. The back-propagating waves of the lower layer are then available for diffraction by the top layer. Both lattices play equally important roles. Suppression of the specular reflection at all angles of incidence is efficiently achieved by the rectangular centred structures in the top layer due to their hexagonal *Brillouin* zone. On the other hand, the long wavelength threshold of the high-reflection bands matches closely the bandgap edge of

the rectangular PC (constructed after average values of the periods) for all angles of incidence and polarisations, while the bandgap edge of the centred rectangular PC is at shorter wavelengths.

It is necessary to consider the effect of disorder in the microstructure to judge the convenience of the modelling with periodic structures. A large change in lateral period does not affect the spectra for wavelengths above the long-wavelength edge of the high-reflection band (cf. section 5.2), but it influences the direction of propagation of the diffraction orders. The direction of propagation of the back-scattered light is determined by the wavelength and the period of the lateral distribution of dielectric. The impinging wave couples to periodic modes in the dielectric which decompose into waves propagating in different directions, each direction determined by the reciprocal lattice vectors. Figure 6.8 illustrates the decomposition of the field within the microstructure and the spread in the directions of propagation caused by the distribution of lateral periods. Considering a distribution of lateral periods ($(675 \pm 175)nm$) to account for the irregularity of the butterfly microstructure shows that a grating-like model, whereby the back-scattered power is organized in orders of diffraction, can account for the microstructure phenomenology. The resulting distribution in the propagation of the orders of diffraction is illustrated in figure 6.4. The peaks of the measured back-scattering overlap the 1^{st}, 2^{nd} and 3^{rd} order of diffraction of a distribution of lateral periods. The progressive angular spread of the orders with increasing angle of propagation – an order propagating at large angles undergoes a larger angular spread than one propagating close to the normal – seems to match the measured spread of the powers scattered by the structure. The waves propagating within the structure are reflected by its layering and couple to back-diffracted waves in the incident medium. A variation of the normal period shifts the band edge proportionally to the value of the period, but does not affect dramatically a scaled spectrum (cf. section 5.2), therefore disorder of the vertical periods mainly causes a reduction in the slope value of the band edge. Deviations from strictly periodic patterns,

for example at the boundary between regular regions of the microstructure, can cause confined states of the coupled waves, which can accumulate and produce high field concentrations. Finally, irregularities in the shape of the small features of the microstructures are expected to cause variations in the *Rayleigh* scattering of the diffracted fields. *Rayleigh* scattering causes a wide angular spread of the diffracted light and is particularly noticeable if the fields are very strongly localized in minute features, a factor that could be related to the widely spread bands found at very short wavelengths. The numerical calculations showed that the highest diffraction efficiencies are found for very short wavelengths, which indicates that higher field intensities exist at those wavelengths within the microstructure and could generate stronger scattering.

Insight has been gained in the role of periodic structures and particular features of the microstructures in the generation of the structural colour. For a complete modelling of the interaction of light with the *Morpho* microstructure, a conclusive assessments of the disorder is necessary and then its rigorous implementation in the model. A structure more closely mimicking the real arrangement can be studied using the FDTD/NFFFT computational tool. A faithful representation should include the central stalk occurring in each tree-shaped diffraction element, the influence of which in the production of colour has not been assessed conclusively in previous studies [25].

In conclusion, let us consider the appearance of *Morpho rhetenor* in its environment. In general, light does not impinge on the scales at normal angles with the ridges. For an arbitrary direction of incidence, the light scattered by the natural grating propagates along directions on the surface of a circular cone, the angle at the vertex of which is determined by the direction of incidence and the orientation of the ridges. This is illustrated in figure 6.9. Only the component of the incident wave vector $\vec{k}_i$ which lies in the plane perpendicular to the ridges and corresponds to the projection of the vector onto it ($\vec{k}_{i\perp}$) influences the interaction of the light with the microstructure. The component parallel to the ridges is conserved: $\vec{k}_{i\parallel} = \vec{k}_{s\parallel}$. The incident

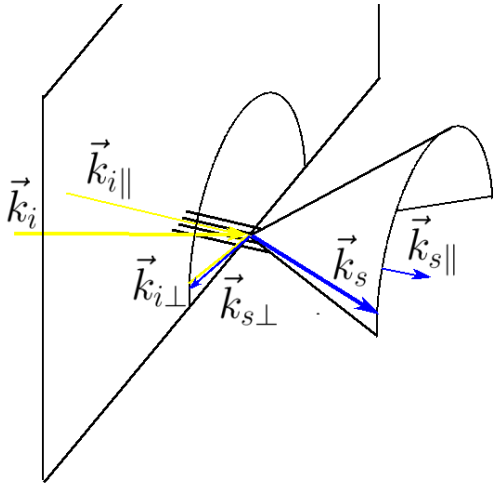

Figure 6.9: Illustration of the interaction of light with the *Morpho* microstructure. The wave vector of the incident wave $\vec{k}_i$ is separated in its components parallel and perpendicular to the ridges, $\vec{k}_{i\|}$ and $\vec{k}_{i\perp}$. The wave vector of the scattered wave $\vec{k}_s$ is equally separated in its components parallel and perpendicular to the ridges, $\vec{k}_{s\|}$ and $\vec{k}_{s\perp}$.

light is mostly scattered into directions close to the mirror image of the direction of incidence with respect to the said plane. The spectral content of the back-scattered light will be mostly blue extending into the green, the intensity of which depends on the polarisation and angle of incidence of the impinging radiation. For light impinging from a specific direction, say from a gap in the forest canopy, the light is filtered and very efficiently scattered collectively by large numbers of scales with the same orientation on the wing of the butterfly. For a fixed observer, this results in strong flashes of blue-green light while the butterfly is flapping its wings. In diffuse light, that is with light impinging on the wing from all directions, the blue-green back-scattered radiation is evenly distributed over the incident hemisphere and its appearance varies only slightly with the direction of viewing.

6.2 Artificial photonic structures inspired by Nature

The optical properties of the *Morpho* microstructure, such as the high diffraction efficiency obtained with a low-index material, the low pass filtering action independent from the angle of incidence, and the strong polarisation dependence of the back-scattered light, are certainly interesting for a variety of applications in photonic engineering. The latest advances in computational photonics allowed studying and identifying the role of various structural features occurring on the butterfly wing. Although an understanding of the mechanisms involved in the optical phenomenology of the microstructure has been reached, it is not possible with the current fabrication technologies to replicate it. Microelectronic fabrication processed widely used in the optoelectronic industry provided the means to produce diffractive structures with vertical and lateral distributions comparable to those in the butterfly microstructure.

A microelectronic fabrication facility is a self-contained, isolated environment where the available processes enable the engineer to reliably structure thin films of silicon-based materials with features on a micron scale. Such miniaturization has been made possible through the development of chemical and physical processes which require the use of high purity substances in an uncontaminated and controlled atmosphere. The dimensional boundaries are constantly being pushed towards smaller sizes due to the ever changing demands of the microelectronic industry. This means, that in recent years the fabrication processes have been optimized to work on yet a smaller scale and state-of-the-art methods now yield features a few hundred nanometers in size.

In this study, common microelectronic fabrication processes have been used to produce novel two- and three-dimensional volume diffractive structures inspired by the *Morpho* microstructure. The devices were designed to operate in the visible spectrum of wavelengths, which entailed the develop-

ment of ultra-high resolution lithographic processes to structure the materials on a nanometer scale. Production of a *Morpho*-type layered arrangement required the development of tightly controlled depositions of thin-films stacks including up to 21 layers, and of anisotropic etching techniques, allowing to etch the stacks with features typically a few hundred nanometer wide and $1.8\mu m$ deep. No such structures have been previously reported. Details about the devices and the fabrication methods employed are presented in chapter 3.

The two-dimensional structures were lamellar gratings with multilayered lamellae, exhibiting a rectangular crystal lattice. They were two-dimensional photonic crystals composed of three dielectrics: two silicon-based amorphous materials and air. A vertical modulation of the index of refraction was achieved through the alternate stacking of thin films of SiO_2 and Si_3N_4 on a substrate, while a horizontal modulation arose from a subsequent etch of trenches into the multilayer on a grating pattern. The definition of small-size openings in the resist was limited by the patterning technique and resulted in the smallest openings having a dimension of about $300nm$. The subsequent etching processes generated an enlargement of the patterned openings and ultimately resulted in smallest etched trenches about $400nm$ wide.

The same fabrication techniques were used to produce the three-dimensional structures. They were produced through patterning the resist with circular openings on a triangular lattice and then etching air columns into the multilayer. The resulting arrangements were three-dimensional photonic crystals with a hexagonal lattice, the well known graphite crystal. All fabricated structures had horizontal periods ranging from 260 to $610nm$, vertical ones of 140 and $175nm$, and the patterned areas were several tens of microns wide.

One fabricated two-dimensional structure was characterised using the optical setup developed for the study of the butterfly microstructure. The measurements are presented in section 4.4. The device had a lateral and a vertical period of 510 and $175nm$, respectively, and an estimated air filling

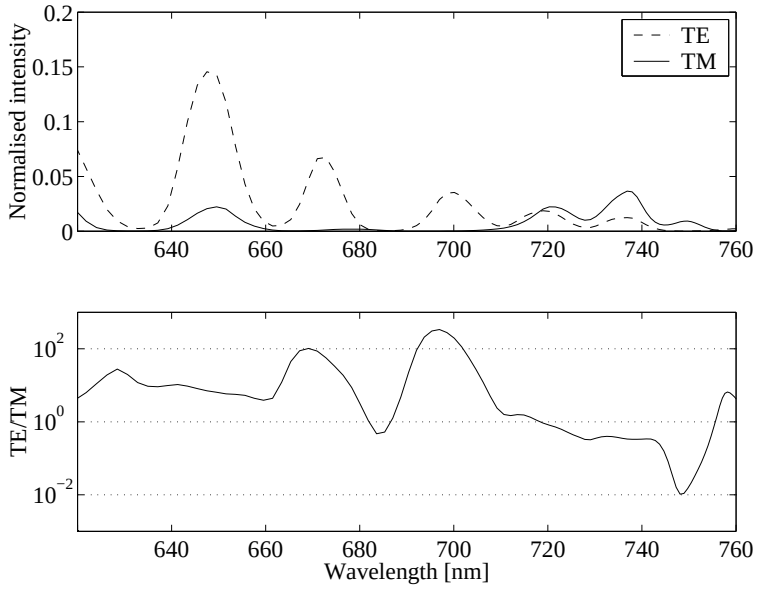

Figure 6.10: Diffraction efficiency of the 1st order for an angle of incidence of 30° and both polarisation (top graph) and relative polarisation extinction ratio in logarithmic scale (bottom graph).

fraction of 80%. The structure was fabricated on a silicon substrate with a SiO_2 buffer layer. The low filling fraction of the dielectrics caused the observed efficiencies to be much smaller than the reflectance of the non etched dielectric mirrors. However, the following interesting properties were found experimentally: (i) strongly modulated spectra of the diffraction orders; (ii) diffraction efficiencies larger than 0.35 and 0.15 for the 0th and 1st order, respectively, at all angles of incidence; and (iii) polarisation extinction ratios up to 340, and larger than 100 for all angles of incidence and for selected wavelengths. The high efficiencies were achieved despite the low dielectric filling fraction of the structure and caused, together with the strong polarisation dependence of the spectra, the remarkable polarisation extinction ratios. Figure 6.10 shows the measured order of diffraction for one angle of incidence and the polarisation extinction that ensues the different modulation of the spectra for the two polarisations.

Both, the strong polarisation dependence and the achievement of comparable diffraction efficiencies at all angles of incidence are properties shared by the characterised device with the *Morpho* microstructure. Numerical computations have shown that for larger dielectric filling fractions much higher diffraction efficiencies can be obtained. The response of the structures however is strongly dependent on the slope of the walls of the diffractive elements.